Direct experimental evidence for the adsorption of 4-tert-butylpyridine and 2,2′-bipyridine on TiO_2 surface and their influence on dye-sensitized solar cells' performance

Phan, Thu Anh Pham; Nguyen, Nghi Phuong; Nguyen, Le Thi; Nguyen, Phu Hoang ; Lea, Tien Khoa ; Huynhb, Tuan Van Huynhb; Lund, Torben; Tsai, De-Hao; Weid, Tzu-Chien ; Nguyen, Phuong Tuyet

Published in:
Applied Surface Science

DOI:
10.1016/j.apsusc.2019.144878

Publication date:
2020

Document Version
Peer reviewed version

Citation for published version (APA):
Phan, T. A. P., Nguyen, N. P., Nguyen, L. T., Nguyen, P. H., Lea, T. K., Huynhb, T. V. H., Lund, T., Tsai, D.-H., Weid, T.-C., & Nguyen, P. T. (2020). Direct experimental evidence for the adsorption of 4-*tert*-butylpyridine and 2,2′-bipyridine on TiO_2 surface and their influence on dye-sensitized solar cells' performance. *Applied Surface Science*, *509*(509), Article 144878. https://doi.org/10.1016/j.apsusc.2019.144878

Direct experimental evidence for the adsorption of 4-*tert*-butylpyridine and 2,2'-bipyridine on TiO_2 surface and their influence on dye-sensitized solar cells' performance

Thu Anh Pham Phan[1#], Nghi Phuong Nguyen[1#], Le Thi Nguyen[1], Phu Hoang Nguyen[1], Tien Khoa Le[1], Tuan Van Huynh[2], Torben Lund[3], De-Hao Tsai[4], Tzu-Chien Wei[4], Phuong Tuyet Nguyen[1*]

[1] *Faculty of Chemistry, University of Science, Vietnam National University Ho Chi Minh City, Vietnam*

[2] *Faculty of Physics and Engineering Physics, University of Science, Vietnam National University Ho Chi Minh City, Vietnam*

[3] *Department of Science and Environment, Roskilde University, Denmark*

[4] *Chemical Engineering Department, National Tsing Hua University, Taiwan R.O.C*

[*] Corresponding author: Phuong Tuyet Nguyen, e-mail: ntphuong@hcmus.edu.vn

[#] Share the first authorship

Key words: dye-sensitized solar cell; 4-*tert*-butylpyridine; 2,2'-bipyridine; TiO_2 adsorption; N-additive

Abstract

We have investigated the binding of two electrolyte additives, 4-*tert*-butylpyridine (4-TBP) and 2,2'-bipyridine (bipy), to the surface of TiO_2 photo-anode by attenuated total reflection – Fourier transform infrared spectroscopy (ATR-FTIR); X-ray photoelectron spectroscopy (XPS); zeta potential; cyclic voltammetry analyses, and explained how the adsorption affects photovoltaic performance of dye-sensitized solar cell (DSC). To clarify

whether the adsorption of 4-TBP/bipy on TiO_2 surface affects the DSC performance, DSC devices were fabricated with non-grafted and 4-TBP or bipy grafted TiO_2 photo-anodes, with application of two types of electrolytes with and without the nitrogen additives. Furthermore, the interaction between 4-TBP or bipy with the electrolyte mediator I^-/I_3^- was investigated by cyclic voltammetry. The results showed that 4-TBP and bipy were able to bind chemically to TiO_2 surface at elevated temperatures. DSC prepared with N-additive grafted TiO_2 photo-anodes had lower short current and efficiencies than non-grafted cells. The open circuit voltage (V_{oc}) was, however, increased 110 mV for 4-TBP grafted cells with 0.5 M 4-TBP in the electrolyte. One third of the overall increase in V_{oc} was estimated to be due to the adsorption of the 4-TBP to the TiO_2 surface. The remaining V_{oc} increase was due to effects of 4-TBP on the electrolyte mediator.

1. Introduction

Dye-sensitized solar cell (DSC), which is known as the third generation of photovoltaic cell, has been extensively studied over the years for its low manufacturing cost and promising power conversion efficiency [1-3]. A DSC cell has three primary parts including a dye attached to a TiO_2 photo-anode, a platinum cathode, and an electrolyte in between the two electrodes. A DSC electrolyte typically consists of an iodide/triiodide (I^-/I_3^-) redox couple, guanidine thiocyanate, and N-additives dissolved in either liquid or ionic liquid as solvents. The commonly used N-additive, 4-*tert*-butylpyridine (4-TBP), has been reported to reduce the dark current between the photo-anode and the oxidized form of the mediator I_3^- by forming a complex between 4-TBP and the mediator [4-7]. More importantly, 4-TBP helped to enhance the open circuit voltage (V_{oc}) of DSC by about 200 mV, and thus increased the power conversion efficiency (η) of the cell by about 1–2% [4-8]. This effect may be due

to the adsorption of 4-TBP molecules on the surface of TiO_2, resulting in a shift of TiO_2 Fermi level to a more negative redox potential [6-9].

However, there have been very few studies that unambiguously support the aforementioned hypotheses. The coordination bond between 4-TBP and TiO_2 was reported elsewhere by either theoretical calculations or experiments [8, 10-13]. By theoretical modeling, Kusama [11] and Xiong [12] suggested that 4-TBP coordinated to TiO_2 through a binding of the N atom in the 4-TBP molecule to the Ti atom. Using ultraviolet photoelectron spectroscopy and absorption and luminescence spectroscopies, Dürr *et. al.* [8] and Katoh *et. al.* [7] showed the adsorption of 4-TBP on TiO_2 surface based on the differences in the spectra and an observed shift of TiO_2 band gap. Yurdakul [10] and Shi [13] provided more experimental evidence for the adsorption of 4-TBP on TiO_2 surface by Fourier transform infrared (FTIR) and Raman spectroscopies, in which the band gap of TiO_2 was shown to shift to a more negative potential. Recently, Johansson *et. al* [14] illustrated the adsorption of 4-TBP on TiO_2 surface by X-ray photoelectron spectroscopy (XPS) in solid state DSC by comparing the spectra with and without 4-TBP; however, its chemically bonds were not analyzed. It is worth noting that the adsorption of 4-TBP on TiO_2 surface was obtained by heating TiO_2 powder in concentrated 4-TBP solution at 200 ^oC for at least two hours [13]. These conditions are very much different from the normal DSC fabrication protocol, where 4-TBP (0.5 M) is added to the electrolyte at ambient temperature. Despite these reports based on both theoretical calculations and experiments, there is no unambiguous evidence of the chemical characteristics of the adsorption of 4-TBP on TiO_2 surface and its direct effect on DSC performance.

Recently, our group has used 2,2'-bipyridine (bipy) instead of 4-TBP as N-additive in DSC electrolyte to minimize the thermal degradation of ruthenium dye (*e.g.* N719) caused by reactions between the dye and 4-TBP [15-17]. The new additive bipy displayed different

effects on the J_{sc} and V_{oc} values from those of 4-TBP when tested in functional DSC devices. We hypothesize that bipy and 4-TBP might be adsorbed onto the TiO_2 surface by different binding modes and thus exert different effects on DSC performance. We report here our investigation of the chemical characteristics of the bonds between the two N-additives and the surface of TiO_2 using FTIR and XPS analyses following heating the TiO_2 powder in bipy or 4-TBP solutions. Moreover, we investigated the effects of the 4-TBP or bipy grafting on the surface potential and electron transfer properties of the TiO_2 electrodes by Zeta potential measurement and cyclic voltammetry analysis, respectively. Furthermore, our study also aimed to provide direct experimental evidence for the influence of N-additive adsorption on DSC photovoltaic performance. In this work, DSC devices containing TiO_2 electrodes grafted with 4-TBP or bipy at various grafting times (0-100 hours) were characterized by *J-V* measurement and cyclic voltammetry.

2. Experimental section

2.1 Materials

Transparent titanium dioxide paste HT/SP, platisol catalyst paste T/SP, and ruthenium N719 dye were from Solaronix (Aubonne, Switzerland). The N-additives which are 4-*tert*-butylpyridine (4-TBP), 2,2'-bipyridine (bipy) and tetrabutylammonium tetrafluoroborate ($TBABF_4$) were purchased from Sigma-Aldrich (S. Louis, MO, USA). Iodine and lithium iodide were from Merck (Damstadt, Germany). Acetonitrile (ACN, high performance liquid chromatography grade) was obtained from Scharlau (Spain). 1,4-dicyanonaphthalene (DCN) was synthesized according to the procedure reported elsewhere [18]. Dupont® Kapton® polyimide film (50 µm thickness) was from RS Components Pty. Ltd. (Denmark). Fluorine-doped tin oxide (FTO) conductive glass substrates (8 $\Omega.cm^{-2}$ conductivity) were purchased from Pilkington.

2.2 Preparation of TiO_2, TiO_2|4-TBP, TiO_2|bipy working electrodes

To prepare the TiO_2 working electrodes, firstly the FTO glass substrates were cleaned with acetonitrile and ethanol and dried at 100ºC for 30 minutes. Then a layer of 0.25-cm^2 TiO_2 HT/SP was deposited on FTO by screen printing. The TiO_2 electrodes were sintered at 500ºC for 30 minutes and cooled down to 80–100ºC before use.

To graft 4-TBP or bipy to TiO_2 surface, the TiO_2 electrodes were immersed in 0.5 M solution of either 4-TBP or bipy in acetonitrile at 80 ºC for 48 to 540 hours. The electrodes were then cleaned by acetonitrile and absolute ethanol several times, and dried under nitrogen flow. In this report, these electrodes are named with the label: TiO_2|N-additive|immersion-time (i.e., TiO_2|4-TBP|48: TiO_2 electrode grafted with 4-TBP for 48 hours).

2.3 Characterization of the adsorption of 4-TBP or bipy on TiO_2 surface

ATR-FTIR measurement

The adsorption of 4-TBP or bipy on TiO_2 surface was determined by the Fourier transmission infrared spectroscopy (FTIR) with a Perkin Elmer FTIR spectrometer 2000 equipped with a PIKE MLRacle ATR accessory.

XPS analysis

The influences of bipy and 4-TBP adsorption on the chemical environment of elements at TiO_2 surface were investigated by the X-ray photoelectron spectra (XPS). These spectra were recorded using a Kratos Axis Ultra-DLD spectrometer (Kratos Analytical Ltd, UK) equipped with a hemispherical analyzer and a monochromatized radiation Al Kα line (1486.6 eV) at 150 W. All the binding energies were referenced to the C 1s peak at 285.0 eV which is attributed to the surface carbon contamination.

Cyclic voltammetry analysis

The effect of the 4-TBP or bipy grafting on the electron transfer from the TiO_2 electrode to a redox probe was investigated by a cyclic voltammetry method developed by T. Lund *et al* [18]. The effect of the surface coating was evaluated by comparing the voltammograms obtained with non-grafted and grafted electrodes in solutions of the redox-probe 1,4-dicyanonaphtalein (2 mM) in a solution of 0.1 M $TBABF_4$ in ACN. The voltammograms were obtained by a standard three-electrode setup with a VersaSTAT 3 potential state (Princeton Applied Research). The working electrode was either a non-grafted TiO_2 electrode or a 4-TBP or bipy grafted TiO_2 electrode with an Ag wire as reference electrode, and a platinum wire as counter electrode. The electrolyte solution was purged carefully with nitrogen prior to each CV measurement.

Zeta potential measurement

Zeta potential (ZP) measurements were performed by a Zeta sizer Nano (Malvern Instruments, Westborough, MA, USA) with a palladium dip cell module at a constant temperature of 25 ˚C. The measured electrophoretic mobility was converted to ZP using the Smoluchowski approximation [19].

Electrospray-differential mobility analysis (ES-DMA) was employed to generate the mono-disperse droplets for the characterization of functionalized TiO_2 in the form of colloidal dispersion [20, 21]. The step size used in the measurements of ES-DMA was 2 nm and the step time was 10 s. Details of ES-DMA are described in the previous publications [20, 21].

2.4 DSC fabrication and characterization

The DSC devices were fabricated following our previously-described procedure [22, 23]. Briefly, 12 μm-thick TiO_2 nanoparticles (Eternal Materials Ltd, R.O.C Taiwan) and 4 μm-thick scattering layer (CCIC, Japan) were screen-printed onto cleaned and $TiCl_4$-treated FTO electrode (Dyesol, 8 $\Omega.cm^{-2}$). After annealing at 500 ºC, the TiO_2 anodes were retreated with 40 mM $TiCl_4$ at 70 ºC for 30 minutes and annealed at 450 ºC for another 30 minutes. The photo anodes were then grafted at 80 ºC in either 0.5 M 4-TBP or 0.5 M bipy solution for different intervals ranging from 0 to 96 hours. Then grafted TiO_2 electrodes were immersed in a dye solution of 0.3 mM di-tetrabutylammonium *cis*-bis(isothiocyanato)bis(2,2'-bipyridyl-4,4'-dicarboxylato) ruthenium(II) (N719, Dyesol, Australia) in dimethyl sulfoxide:ethanol (1:9, v/v) for 12 hours. The grafted and dye-soaked TiO_2 electrodes were then assembled with platinized-FTO counter electrodes. Finally, electrolyte solutions were injected into the devices and sealed carefully.

To investigate the influence of the N-additives dissolved in the DSC electrolyte , 0.5 M of 4-TPB or bipy was added to the electrolyte of 0.05 M LiI, 0.5 M TBAI, and 0.05 M I_2 in ACN. A DSC prepared with an electrolyte without N-additives was used as a control. Photovoltaic performance of DSC was characterized by *J-V* measurements by a model 2400 digital source meter (Keithley, USA), under a solar simulator AM 1.5 (1,000 $W.m^{-2}$) using 450 W xenon lamp, following the protocol as described elsewhere [24]. The DSC devices were masked with a 0.1444 cm^2 active area of the photo-anode.

2.5 CV analysis of interaction between 4-TBP or bipy with redox mediator I^-/I_3^-

For a more detailed understanding of the effects of N-additives on the DSC performance, we investigated the interaction between 4-TBP or bipy with the redox couple I^-/I_3^-. Cyclic voltammetry measurements were obtained by a Metrohm Autolab potentiostate

and a standard three-electrode electrochemical cell composed of a platinum working electrode, a platinum wire as counter electrode and a silver wire as reference electrode. The experiments were performed with electrolyte solutions comprised of 100 mM LiI in ACN supplemented with various concentrations of 4-TBP or bipy (0, 10, 50, 500 mM). The supporting electrolyte was prepared with 0.1 M $LiClO_4$ in ACN. All the solutions were purged carefully by nitrogen before CV measurement. The scan rate was set at 50 mV/s.

3. Results and discussion

3.1 Adsorption of 4-TBP or bipy on TiO_2 surface

ATR-FTIR analysis

The IR spectra of bare and grafted TiO_2 electrodes were shown in Figure 1. The peaks at 1596, 1544 and 1494 cm^{-1} of pure 4-TBP were assigned to pyridine (py) ring stretching vibrations (dark green curve in fig. 1a). Additionally, the CH_3 asymmetric vibrations of *tert*-butyl were identified at 1469, 1457, 1409, 1365 cm^{-1}; and C—N stretching in pyridine ring at 1280 cm^{-1}. In the spectra of TiO_2 grafted 4-TBP, a broad peak at 1650 cm^{-1}, a small peak at 1409 cm^{-1}, a peak at 1337 cm^{-1} were observed and became sharper. The peak intensities increased when the adsorption time was longer. These peaks indicated the adsorption of 4-TBP on TiO_2. The pyridine stretching signals (1652, 1642, 1587 cm^{-1} in red curve) of the sample TiO_2|4-TBP were shifted to higher wavenumbers; and the appearance of new signal at 1617 cm^{-1} confirmed the chemical adsorption of 4-TBP on TiO_2 by Ti-N coordination [13]. Furthermore, the CH_3 vibrations were relocated at 1422, 1400, 1365, 1337 cm^{-1}. Compared with pure 4-TBP vibration signals, the wavenumber of the pyridine ring and CH_3 vibrations of TiO_2|4-TBP|144h sample were shifted 28-98 cm^{-1} to higher values. The shift of wavenumbers to higher values indicates an increase of the force constant of the pyridine

molecule, which may be explained by the formation of Ti-N bonds [13]. In addition, we observed two large shoulder bands at 876-793 and 776-528 cm^{-1} and a medium signal at 781 cm^{-1} (fig. 1b), which were not present in bare TiO_2 spectra. These shoulders might be due to the adsorption of 4-TBP. The changes in the spectral interval 700-800 cm-^{1}, identified as the region of Ti-O vibrations, may be explained by the impact of Ti-O-N bond formation [25].

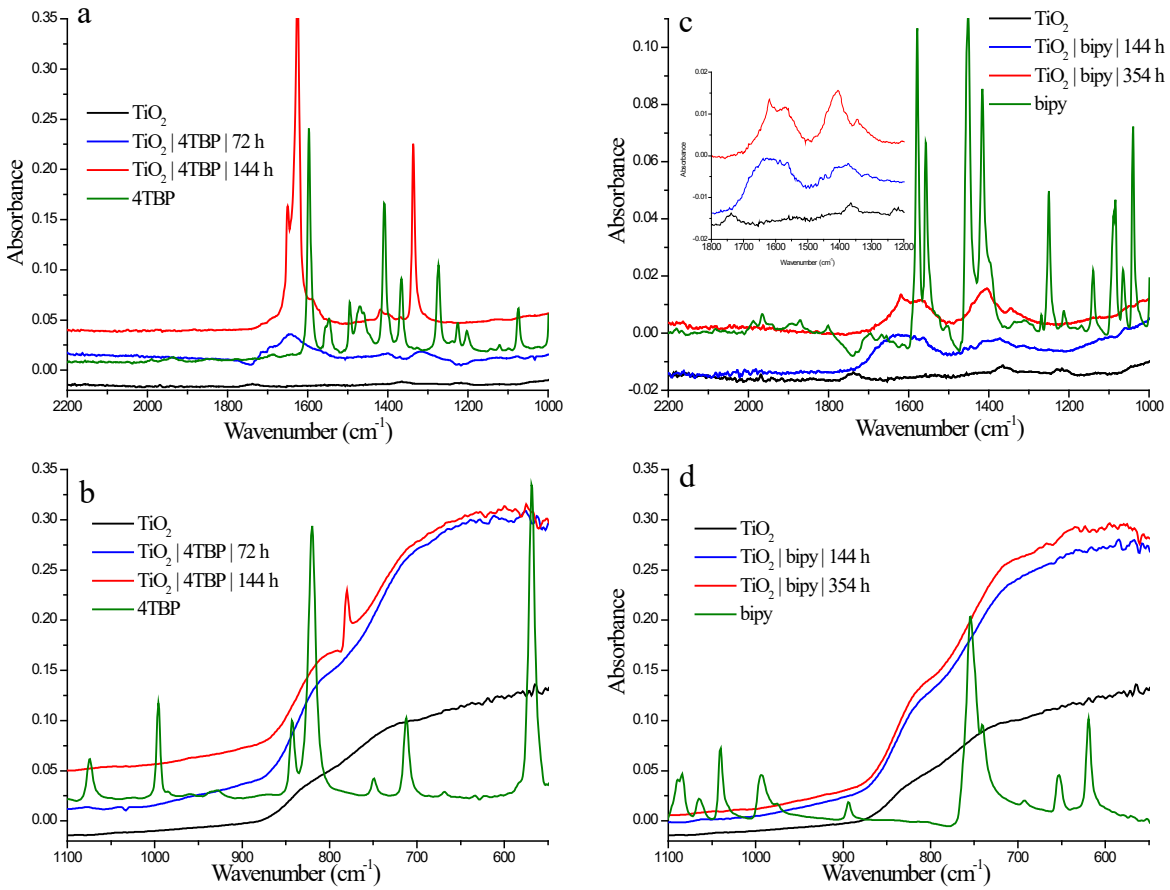

Figure 1. Infrared spectra of (a, b) TiO_2|4-TBP; (c, d) TiO_2|bipy with various adsorption time compared to the bare TiO_2 sample. The figures in (a) and (c) represent the spectra with the wavenumber from 1000 to 2200 cm^{-1}, while (b) and (d) from 550 to 1100 cm^{-1}.

The signals of TiO_2|bipy spectra were not as sharp and strong as the resonances of the 4-TBP samples. The spectrum of the TiO_2|bipy|354h sample (red curve, fig. 1c), showed four broad pyridine ring stretching vibrations at 1629, 1590, 1410, 1340 cm^{-1}. The 1629

and 1590 cm^{-1} peaks were shifted to higher frequencies compared with pure bipy, whereas the 1410 and 1340 peaks were lowered by 40-60 $cm^{-1.}$. The shift changes may be explained by the difficulty of bipy adsorption on TiO_2 due to its bulky geometry-constrained structure. The molecular structure of bipy does only allow one of its pyridine rings to react with TiO_2 resulting in a change of force constant between two py rings. The samples with low bipy grafting time showed broad band which became sharpened at larger grafting times. This can be explained by a higher amount of bipy adsorbed to the TiO_2 surface leading to the stronger vibrations of featured bonds. As previously discussed [25, 26], we also suggest that bipy is adsorbed on TiO_2 by Ti-N or/ and Ti-O-N bonds. This hypothesis is also supported by the two broad shoulder bands at about 500-780 and 780-880 cm^{-1} in the fingerprint region which were different from bare TiO_2 and pure bipy spectra.

To conclude, 4-TBP and bipy were adsorbed on TiO_2 surface through Ti-N or/ and Ti-O-N bonds and the amount of adsorbed 4-TBP or bipy increased as a function of loading time.

XPS analysis

The surface elemental composition of TiO_2, TiO_2|4-TBP|time, and TiO_2|bipy|time samples, and the chemical environment of C, Ti, O and N atoms on their surface were reported in Table 1. Figure 2 (left top) presents the high resolution XPS spectra of C 1s region, taken on the surface of our materials. The bare TiO_2 sample shows an asymmetrical peak, which can be deconvoluted to three components. The most intense component situated at 285 eV is assigned as C-C and C-H bonds whereas the two minor peaks at 286.6 and 288.9 eV were attributed to C-O and O=C-O bonds originated from surface contamination carbon [27]. We observed that the chemical environment of carbon on TiO_2 surface was not

significantly affected after the adsorption of bipy, but strongly modified after the adsorption of 4-TBP. In fact, two new peaks were detected at 288.3 eV and 292.1 eV in the high resolution C 1s spectra of TiO_2|4-TBP|time. Since the intensity of the C 1s peak situated at 288.3 eV was three times more intense than the C 1s peak at 292.1 eV, the former peak and the latter peak should be assigned to C-C and C-N bonds in the adsorbed 4-TBP molecules, respectively.

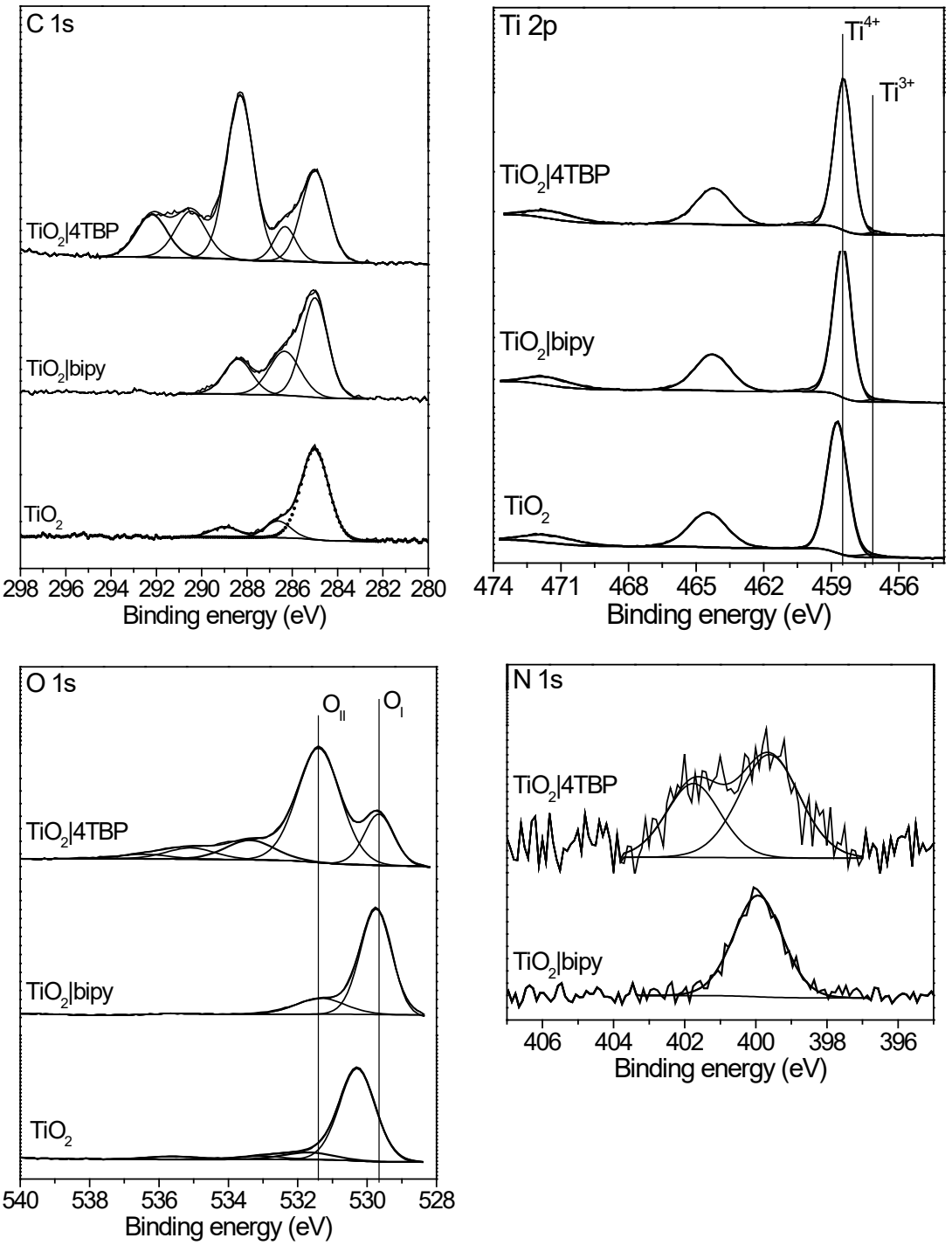

Figure 2. XPS analysis of (a) C 1s; (b) Ti 2p; (c) O 1s; and (d) N 1s of the TiO_2|4-TBP; TiO_2|bipy samples compared to the bare TiO_2

Table 1. High resolution XPS data of bare TiO_2, TiO_2|4-TBP and TiO_2|bipy samples

		C 1s				Ti^{4+} $2p_{3/2}$-$2p_{1/2}$	Ti^{3+} $2p_{3/2}$	O1s I	O1s II	O1s III	O1s IV	O1s V	N1s I	N1s II	O_{II}/Ti	Ti^{3+}/Ti^{4+}	N/Ti
TiO_2	B.E. eV (FWHM)	285.0 (1.4)	286.5 (1.3)	288.6 (1.6)		458.7-464.5 (1.0-1.09)	457.3 (0.7)	535.6 (1.6)	531.7 (1.6)	533.0 (1.5)	535.6 (1.6)				0.24	0.016	
	%	12.67	2.16	1.48		22.63	0.37	2.17	5.46	2.22	2.17						
TiO_2 | 4-TBP	B.E. eV (FWHM) eV	285.0 (1.3)	286.4 (1.6)	288.6 (1.3)	290.5 (1.6)	458.4-464.2 (0.9-1.8)	457.0 (0.8)	535.7 (1.6)	531.7 (1.4)	533.4 (1.6)	535.7 (1.6)	536.4 (1.6)	399.3 (1.9)	401.3 (1.9)	6.22	0.011	0.136
	%	8.30	2.53	15.18	4.85	5.64	0.06	3.92	35.12	6.83	3.92	1.59	0.47	0.30			
TiO_2 | bipy	B.E. eV (FWHM) eV	285.0 (1.3)	286.3 (1.6)	288.4 (1.4)		458.5-464.3 (1.0-1.9)	457.0 (1.0)	529.7 (1.0)	531.3 (1.65)				399.9 (1.6)		0.47	0.012	0.070
	%	11.40	6.09	4.35		21.9	0.26	44.02	10.44				1.53				

The high resolution Ti 2p spectra of three samples were exhibited in the Figure 2 (right top). Due to the effect of spin-orbit coupling, TiO_2 always displayed two main peaks at 458.7 and 464.5 eV, followed by a charge-transfer satellite peak at 471.5 eV, which are characteristic for the binding energies of Ti^{4+} in TiO_2 lattice [28, 29]. We also observed a minor peak at 457.3 eV, which may be attributed to the Ti^{3+} ions located in the surface oxygen vacancies of TiO_2 [30]. When 4-TBP or bipy molecules were adsorbed on TiO_2 surface, the molar ratio of Ti^{3+} to Ti^{4+} ions was reduced (Table 1), corresponding to the decrease of Ti^{3+} content. This indicates that during the adsorption process, the 4-TBP or bipy molecules were able to bind to Ti^{3+} ions in the oxygen vacancies, which is in good agreement with the work of Göthelid *et. al* [30].

Therefore, in order to better understand the interactions of adsorbed molecules on the surface of TiO_2, the high resolution O 1s spectra of TiO_2, TiO_2|4-TBP|time and TiO_2|bipy|time were also recorded (Figure 2, left bottom). For the bare TiO_2 sample, the asymmetrical O 1s core peak can be deconvoluted to four components: 530.3 (O_I), 531.7 (O_{II}), 533.0 eV (O_{III}) and 535.6 eV, corresponding to the TiO_2 lattice oxygen [31], OH groups [32] adsorbed H_2O molecules [33] and some C-O bounds, respectively. After the adsorption of bipy molecules, the O_{III} 1s and O_{IV} 1s peaks disappeared, the position of O_I 1s and O_{II} 1s peak shifted to the lower binding energy and the intensity of O_{II} 1s peak significantly increased. Since the bipy molecule does not contain oxygen atom, the increase in O_{II} 1s intensity may not originate from the enhancement of OH groups but from the interaction between bipy molecules and oxygen species on TiO_2 surface. Likewise, when 4-TBP molecules were absorbed on TiO_2 surface, the binding energy of O_I 1s peak decreased, the intensity of O_{II} 1s component (531.7 eV) was greatly enhanced and a new O1s peak appeared at 536.4 eV. These modifications indicate that the adsorption of bipy and 4-TBP most likely

occur on the surface oxygen sites via the Ti-O-N bonds, which was also suggested by the FT-IR results.

However, the content and the chemical environmental of adsorbed 4-TBP molecules should be different from those of adsorbed bipy molecules. In fact, for the TiO_2|bipy|time, the N 1s spectrum only shows one peak at 399.9 eV whereas the N 1s spectrum of TiO_2|4-TBP|time presents two peaks at 399.3 and 401.3 eV (Figure 2 right bottom). In the literature, the N 1s core peak at 399–400 eV usually originates from the nitrogen species bound to various surface oxygen sites [34] such as N-O bonds [35] or Ti-O-N bond [36]. It has also been reported that the N 1s peak at 401.3 eV could be attributed to the O-Ti-N linkage [37] or Ti-N-O linkage [38]. Therefore, we believe that the adsorption of 4-TBP could occur through the formation of both Ti-N and O-N bonds. Moreover, the molar ratio of N atoms to Ti^{4+} ions in the TiO_2|4-TBP|time sample was found to be two times higher than that in TiO_2|bipy|time sample. Based on the content of N and C atoms on the surface of these samples, it is reasonable to conclude that 4-TBP is more readily absorbed on the TiO_2 surface than bipy. The binding of 4-TBP or bipy on TiO_2 surface can be summarized as in diagram 1.

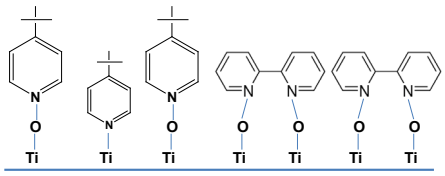

Diagram 1. Model of 4-TBP or bipy binding to TiO_2 surface. 4-TBP can bind to TiO_2 surface through both Ti-N and Ti-O-N bonds while bipy can bind to TiO_2 by mostly Ti-O-N bonds.

3.2 Cyclic voltammetry analysis

We have recently developed a cyclic voltammetry method to study the blocking effect of 4-TBP or bipy grafted TiO_2 electrodes [18, 24, 39]. 1,4-dicyanonaphtalene (DCN) with a

E^o = -1.5 V vs. SCE , was used to investigate the heterogeneous electron transfer kinetics between DCN and the surface coated TiO_2 electrodes.

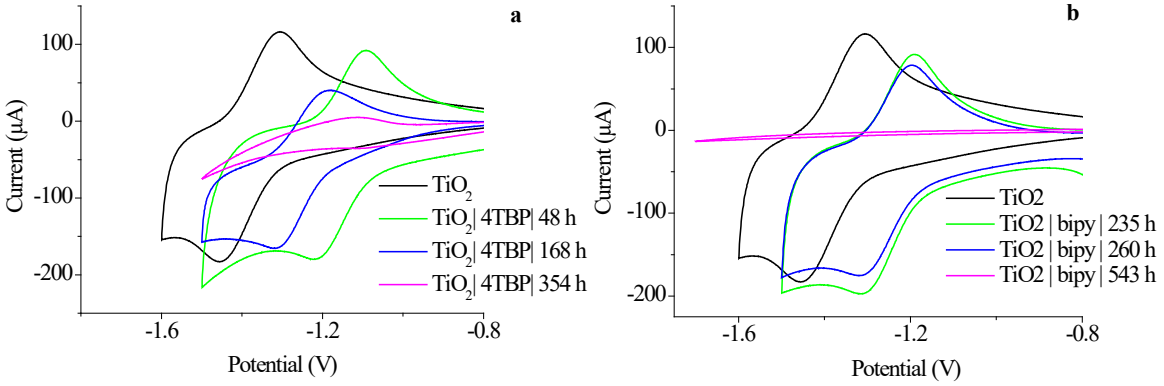

Figure 3. Cyclic voltammograms of 2 mM DCN in 0.1 M $TBABF_4$ at a scan rate of 0.02 Vs^{-1} with different working electrodes: TiO_2, TiO_2|4TBP|time (a), TiO_2|bipy|time (b).

Figure 3a, 3b present the reversible cyclic voltammograms of DCN with TiO_2|4-TBP and TiO_2|bipy as working electrodes, respectively, in comparison with the bare TiO_2 electrode. The anodic and cathodic peaks of the DCN voltammograms were shifted to more positive potentials compared with the bare TiO_2 electrode. The observed cathodic shift is a consequence of reduce heterogeneous electrode.

When using TiO_2|4-TBP, after 354 hours of adsorption, the anodic and cathodic peak currents of DCN practically disappeared (Fig. 3a, pink curve), supporting the ultimate blocking ability of electron kinetics of 4-TBP on TiO_2 electrode surface after a long grafting time at 80 ºC. The same effect was observed when using TiO_2|bipy as working electrode, however, the electrodes needed longer grafting time of bipy to obtain the blocking layer effect as 4-TBP. This low capability of blocking electron transport onto TiO_2 surface can be explained by the bulky geometry-constrained structure of bipy explains why the full blocking layer of the TiO_2 surface is established more slowly than for 4-TBP.

3.3 Zeta potential measurement

Zeta potential (ZP) measurement and electrospray-differential mobility analysis (ES-DMA) were employed to investigate the presence of corona (4-TBP, bipy) on the surface of TiO_2. Figure 4a shows the ZP profiles of TiO_2, TiO_2|4TPB and TiO_2|bipy versus pH. In comparison to the bare TiO_2, the absolute value of zeta potential of TiO_2|4-TBP and TiO_2|bipy decreased by 5–10 mV, implying that the surface of TiO_2 were coated by 4-TBP and bipy, respectively. From the mobility size distributions measured by ES-DMA (Figure 4b), the peak mobility diameter increased from ≈46 nm to ≈52 nm after the coating with both 4-TBP and bipy. The changes of mobility size indicate a conformational change of TiO_2 nanoparticles (i.e., becoming a more open structure agglomerate), confirming that both 4-TBP and bipy were successfully bound to the surface of TiO_2. It is worth noting that the isoelectric points of the three samples remained relatively constant at 5.5–6.0.

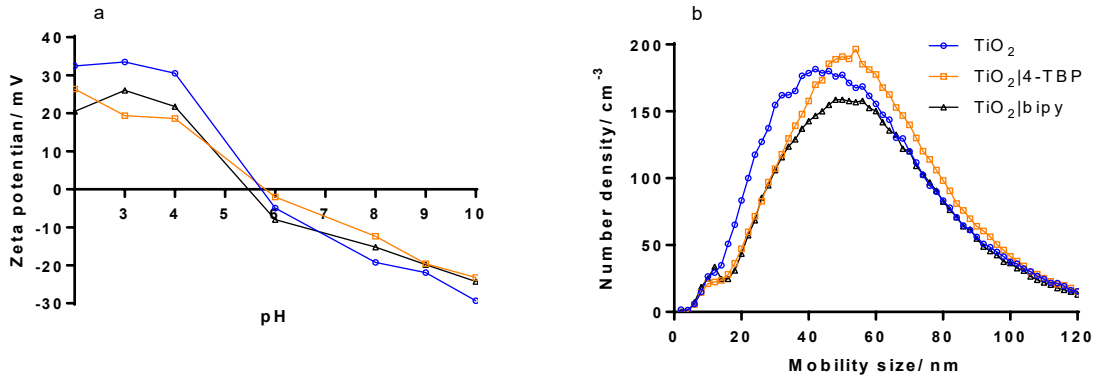

Figure 4. (a) Zeta potential and (b) electrospray-differential mobility analyses of bare TiO_2, TiO_2|4-TBP, and TiO_2|bipy dispersed in water.

3.4 Reaction of 4-TBP or bipy with I^-, I^-/I_3^-

Cyclic voltammetry analysis of the iodide solutions with increasing concentrations of 4-TBP or bipy showed the typical redox behavior of iodide electrochemistry, characterized through a black curve (Fig. 5a and 5b). Here we observed two pairs of oxidation and reduction peaks of the overall process.

$3I^- \rightleftharpoons I_3^- + 2e$ at 0.65 V (1)

$2I_3^- \rightleftharpoons 3I_2 + 2e$ at 1.11 V (2)

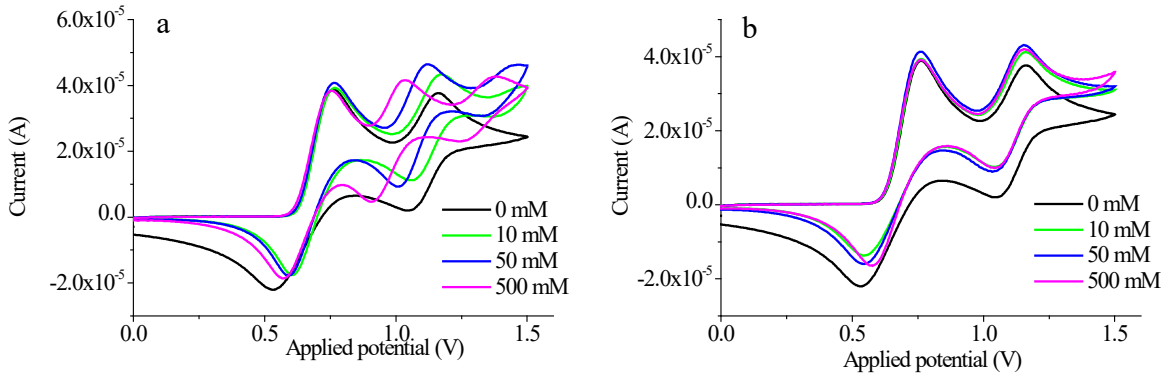

Figure 5. Cyclic voltammograms with ν = 100 mV/s of LiI (100 mM) in a solution of 0.1 M $LiClO_4$ in acetonitrile with addition of (a) 0–0.5 M 4-TBP; (b) 0–0.5 M bipy.

The peak potentials of the first redox pair of eq. (1) are unaffected by the addition of 4-TBP whereas the second pair of peak potentials of eq. (2) were shifted to more positive potentials by ~0.14 V with [4-TBP] = 0.5 M. A small reversible peak appeared at around +1.3 V with increasing peak current with increasing 4-TBP concentrations (Fig. 5a). In contrast, as shown in Fig. 5b, the addition of bipy to the iodide solution did not produce any effects on its CV with neither a shifting of the first or second peak nor an appearance of the third one.

Boschloo *et. al.* have previously made a similar observation of the shifted second peak of the redox couple eq. (2) [4]. They explained the shift as a result of a complexation between iodine and 4-TBP. Nevertheless, Hansen *et.al* demonstrated that 4-TBP and iodine reacts with formation of a idonium complex $(4\text{-TBP})_2I^+,I_3^-$ and not a charge transfer complex $(4\text{-TBP})I_2$ as suggested by Boshloo *et. al.* [40]. We suggested that the shifted second peak and the appearance of the third peak are due to the formation of an iodonium product $(4\text{-TBP})_2I^+,I_3^-$ between iodine and 4-TBP instead of the complexation. Bipy did not have any interaction with the mediator. However, it is of important to notice that the addition of 4-TBP or bipy did not change the redox potential of iodide/ triiodide. This raised the question of how the addition of 4-TBP helped to enhance the V_{oc} values. It was reported by Durrant and co-workers that electron recombination with iodine was much faster than with triiodide [41]. The relation between V_{oc} and k_{rec} can be determined by the following equation.

$$k_{rec} = k^o \exp(-\alpha V_{oc} q/kT)$$

where k^o is the standard rate constant, α is the transfer coefficient varied from 0 to 1 depending on the symmetry of the energy barrier, and q is the elementary charge. Based on the equation, the increase of V_{oc} can be explained as a result of the decrease of electron recombination in the solar cells. The formation of iodonium salt between 4-TBP and iodine could help to reduce iodine concentration and therefore decrease electron recombination rate (k_{rec}) in the DSC devices. On the other hand, Boschloo further suggested that 4-TBP affected the surface charge of TiO_2 by decreasing the amount of proton or Li^+ ion, thereby decreased the accessibility of triiodide toward TiO_2 surface. This effect also helped to reduce the electron recombination and to enhance the V_{oc}.

In summary, the formation of iodonium salt or the effect of 4-TBP on the surface charge of TiO_2 helped to reduce the electron recombination and thus enhanced the V_{oc} significantly (70–100 mV).

3.5 Photovoltaic performance of the DSC

Effects of the adsorption of N-additives on Photovoltaic performance of the DSC

A series of DSC´s were prepared with TiO_2 photo anodes grafted in 0.5 M 4-TBP or bipy solutions for 0 – 96 hours at 80 ºC. The cells were filled with electrolyte A with no additives or electrolyte B with either 0.5 M 4-TBP or bipy. Figure 6 shows the current density – voltage (J – V) curves of four selected cells including the ones with or without the adsorption of 4-TBP on TiO_2 electrodes, simultaneously use A and B electrolytes. It is complicated to show all the J – V curves of all the devices in the figure. Hence, the photovoltaic parameters, including short circuit current density (J_{sc}), open circuit voltage (V_{oc}), fill factor (FF), and overall conversion efficiency (η) of the aforementioned DSC devices were compared (See Table 2).

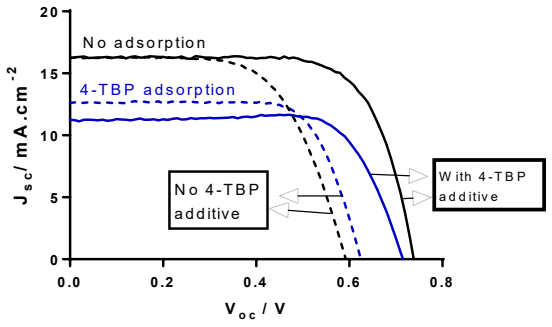

Figure 6. J – V curves of four selected DSC devices using bare TiO_2 (black) or TiO_2 | 4-TBP-30 (blue) photo-anode with electrolyte A (solid line —) or electrolyte B (dash line ---).

Table 2. Photovoltaic performance of DSC devices fabricated with bare TiO_2; various grafted TiO_2 photo-anode by 4-TBP or bipy, in combination with two types of electrolytes A and B.

Electrolyte	**A/ [N-additive] = 0 M**				**B/ [4-TBP] = 0.5 M**			
Adsorption condition	J_{sc} $mA.cm^{-2}$	V_{oc} V	FF	η %	J_{sc} $mA.cm^{-2}$	V_{oc} V	FF	η %
No adsorption	16.24	0.59	0.66	6.32	16.16	0.71	0.73	8.32
TBP-3	16.60	0.54	0.70	6.27	14.24	0.62	0.74	6.54
TBP-6	15.90	0.56	0.71	6.32	13.45	0.62	0.74	6.19
TBP-24	15.14	0.54	0.69	5.63	10.60	0.71	0.75	5.64
TBP-30	12.32	0.63	0.73	5.67	11.37	0.70	0.75	5.97
TBP-75	11.41	0.64	0.75	5.46	9.90	0.70	0.77	5.34
TBP-96	10.52	0.63	0.70	4.64	8.86	0.70	0.77	4.78
Bipy-3	16.69	0.59	0.68	6.75	14.04	0.68	0.69	6.55
Bipy-6	15.92	0.59	0.69	6.52	13.23	0.66	0.70	6.11
Bipy-24	13.03	0.65	0.72	6.14	13.16	0.71	0.75	7.00
Bipy-30	13.25	0.66	0.74	6.47	11.37	0.72	0.76	6.23
Bipy-75	12.45	0.64	0.74	5.90	10.49	0.74	0.76	5.90
Bipy-96	11.56	0.65	0.70	5.26	10.60	0.74	0.73	5.73

The $J - V$ curves in Fig. 6 shows the same shape, indicating similar photovoltaic performance for all the devices. It is obvious that addition of 4-TBP in the electrolyte increased the value of V_{oc} significantly whether or not the TiO_2 adsorbed 4-TBP. As seen from Table 2 the most striking effect of the surface grafting is the drop in the DSC efficiencies η caused by a decrease in J_{sc}. The longer grafting time the larger decrease of J_{sc} and η. The same effect was observed when the photo-anodes were grafted with diazonium or iodonium salts [42]. Grafting of the TiO_2 surface with an organic insulator is in general not a good idea because it introduces a series resistance towards the injection of the electrons to the conduction band with a lowering of J_{sc} as a result. Surface grafting with an insulator may only be when certain one-electron transfer mediators *e.g.* ferrocene are applied as mediator in order to reduce back

electron transfer losses [43]. However, the adsorption of 4-TBP or bipy on TiO_2 surface did improve the fill factor values which slightly increased when electrolyte additive was applied. The 4-TBP or bipy molecules might have a positive effect on the interface between electrodes and electrolyte components in the devices leading to higher fill factor [44, 45].

When the A-electrolyte ([4-TBP] = 0 M) is applied there is a small 40 mV increase in V_{oc} from 0.59 to 0.63 V between a DSC prepared with a non-grafted photoanode relative to a DSC with a 96 hour 4-TBP grafted surface (TBP-96). A similar increase of 60 mV was observed for the bipy grafted DSC (bipy-75). Adding 0.5 M 4-TBP to the electrolyte increases V_{oc} 70 mV from 0.63 to 0.70 V. The combined increase in V_{oc} is 110 mV for 4-TBP and 160 mV for bipy. This means that in the case of 4-TBP (40/110)×100% = 36% of the total V_{oc} increase is related to the binding of 4-TBP on the TiO_2 surface. The remaining 64% V_{oc} increase is due to other reasons. From Table 2 it is seen that a similar increase in V_{oc} is observed (120 mV) in DSC´s prepared the usual way just by adding 4-TBP to the electrolyte without surface grafting. The 4-TBP is in standard DSC preparations most likely physical absorbed to the outer layer of the TiO_2 photo-anode, whereas in the grafting preparation method the 4-TBP has most likely diffused inside the bulk part of the TiO_2 nano particles with formation of thicker layer of 4-TBP with formation of chemical bonds between 4-TBP and TiO_2 as described in the FT-IR and XPS sections. It is, however, the 4-TBP bond to the outer TiO_2 surface which push the conduction band level to more negative potentials [10, 13] and not the binding of 4-TBP several nm inside the TiO_2 nano-particle. In the "no adsorption" case we hypothesize that the effect of 4-TBP physical absorbed on the TiO_2 surface can maximum be as high as the effect of the heavily grafted (TBP-96) photoanode – namely ~40 mV. That means that (40/120)×100% = 30% of the V_{oc} increase of standard DSC containing 0.5 M 4-TBP is due to the surface effect. Several reports [6-13] ascribe the V_{oc} increase to the change of the conduction band level in TiO_2 to more negative potentials by

the 4-TBP adsorption on the TiO_2 surface (Mechanism 1). However, in our work ~70% of the V_{oc} increase is related to the N-additive effects on the electrolyte: Reduction of the back electron transfer loss from the conduction band to I_3^- due to a reduction of the free concentration of I_3^- by complexations with 4-TBP and formation of an iodonium complex (Mechanism 2) [40]; and perturbation of the $3I^- \rightleftharpoons I_3^- + 2e^-$ redox potential by 4-TBP (Mechanism 3).

The CV results here (see section 3.4) and in the work of Boschloo´s *et al.* [4] show that the standard potential of I_3^-/I^- mediator is not affected by 4-TBP. Therefore the V_{oc} increase of 120 mV is most likely a combined effects of TiO_2 | 4-TBP bonding (30%) and 4-TBP/I_3^- complexation.

4. Conclusion

We demonstrated an efficient way to chemically graft 4-*tert*-butylpyridine (4-TBP) and 2,2'-bipyridine (bipy) on the surface of TiO_2. The binding between the bipy and the TiO_2 surface mainly occurred via a Ti-O-N linkage, whereas the binding between the 4-TBP and the TiO_2 surface was via both Ti-O-N and Ti-N bonds. DSC cells prepared with N-additive grafted TiO_2 photo-anodes had lower short current and light to electricity efficiencies than non-grafted cells. The open circuit voltage (V_{oc}) was, however, increased 110 mV for 4-TBP grafted cells with 0.5 M 4-TBP in the electrolyte. One third of the overall increase in V_{oc} was estimated to be due to the adsorption of the 4-TBP to the TiO_2 surface. The remaining V_{oc} increase was attributed to effects of 4-TBP on the electrolyte. We have proposed that the electrolyte effect is due to a reduction of the free I_3^- concentration by complexation with 4-TBP and reduction of the back electron transfer loss reaction from the conduction band to I_3^-.

Acknowledgements

This research is funded by Vietnam National University Ho Chi Minh City under grant number C2018-18-10.

References

[1] L.M. Peter, The Grätzel Cell: Where Next?, J. Phys. Chem. Lett. 2 (2011) 1861-1867. https://doi.org/10.1021/jz200668q

[2] B. O'Regan, M. Grätzel, A low-cost, high-efficiency solar cell based on dye-sensitized colloidal TiO_2 films, Nature. 353 (1991) 737-740. https://doi.org/10.1038/353737a0

[3] A. Hagfeldt, G. Boschloo, L. Sun, L. Kloo, H. Pettersson, Dye-Sensitized Solar Cells, Chem. Rev. 110 (2010) 6595-6663. https://doi.org/10.1021/cr900356p

[4] G. Boschloo, L. Häggman, A. Hagfeldt, Quantification of the Effect of 4-tert-butylpyridine Addition to I^-/I_3^- Redox Electrolytes in Dye-Sensitized Nanostructured TiO_2 Solar Cells, J. Phys. Chem. B. 110 (2006) 13144-13150. https://doi.org/10.1021/jp0619641

[5] H. Kusama, Y. Konishi, H. Sugihara, H. Arakawa, Influence of alkylpyridine additives in electrolyte solution on the performance of dye-sensitized solar cell, Sol. Energy Mater. Sol. Cells. 80 (2003) 167-179. https://doi.org/https://doi.org/10.1016/j.solmat.2003.08.001

[6] V. Gondane, P. Bhargava, Tuning flat band potential of TiO_2 using an electrolyte additive to enhance open circuit voltage and minimize current loss in dye sensitized solar cells, Electrochim. Acta. 209 (2016) 293-298. https://doi.org/https://doi.org/10.1016/j.electacta.2016.05.079

[7] R. Katoh, M. Kasuya, S. Kodate, A. Furube, N. Fuke, N. Koide, Effects of 4-tert-Butylpyridine and Li Ions on Photoinduced Electron Injection Efficiency in Black-Dye-Sensitized Nanocrystalline TiO_2 Films, J. Phys. Chem. C. 113 (2009) 20738-20744. https://doi.org/10.1021/jp906190a

[8] M. Dürr, A. Yasuda, G. Nelles, On the origin of increased open circuit voltage of dye-sensitized solar cells using 4-tert-butylpyridine as additive to the electrolyte, Appl. Phys. Lett. 89 (2006) 061110. https://doi.org/10.1063/1.2266386

[9] S. Zhang, M. Yanagida, X. Yang, L. Han, Effect of 4-tert-butylpyridine on the Quasi-Fermi Level of Dye-Sensitized TiO_2 Films, Appl. Phys. Express. 4 (2011) 042301. https://doi.org/10.1143/apex.4.042301

[10] S. Yurdakul, M. Bahat, Fourier transform infrared and Raman spectroscopic studies on 4-tert-butylpyridine and its metal(II) tetracyanonickelate complexes, J. Mol. Struct. 412 (1997) 97-102. https://doi.org/https://doi.org/10.1016/S0022-2860(96)09392-1

[11] H. Kusama, H. Orita, H. Sugihara, DFT investigation of the TiO_2 band shift by nitrogen-containing heterocycle adsorption and implications on dye-sensitized solar cell performance, Sol. Energy Mater. Sol. Cells. 92 (2008) 84-87. https://doi.org/https://doi.org/10.1016/j.solmat.2007.09.004

[12] B.-T. Xiong, B.-X. Zhou, Z.-Y. Zhu, T. Gao, L.-H. Li, J. Cai, W.-M. Cai, Adsorption of 4-tert-butylpyridine on TiO_2 Surface in Dye-Sensitized Solar Cells, Chin. J. Chem. 26 (2008) 70-76. https://doi.org/10.1002/cjoc.200890040
[13] C. Shi, S. Dai, K. Wang, X. Pan, F. Kong, L. Hu, The adsorption of 4-tert-butylpyridine on the nanocrystalline TiO_2 and Raman spectra of dye-sensitized solar cells in situ, Vib. Spectrosc. 39 (2005) 99-105. https://doi.org/https://doi.org/10.1016/j.vibspec.2005.01.002
[14] L. Yang, R. Lindblad, E. Gabrielsson, G. Boschloo, H. Rensmo, L. Sun, A. Hagfeldt, T. Edvinsson, E.M.J. Johansson, Experimental and Theoretical Investigation of the Function of 4-tert-butylpyridine for Interface Energy Level Adjustment in Efficient Solid-State Dye-Sensitized Solar Cells, ACS Appl. Mater. Interfaces. 10 (2018) 11572-11579. https://doi.org/10.1021/acsami.7b16877
[15] P. Tuyet Nguyen, R. Degn, H. Thai Nguyen, T. Lund, Thiocyanate ligand substitution kinetics of the solar cell dye Z-907 by 3-methoxypropionitrile and 4-tert-butylpyridine at elevated temperatures, Sol. Energy Mater. Sol. Cells. 93 (2009) 1939-1945. https://doi.org/https://doi.org/10.1016/j.solmat.2009.07.008
[16] P. Tuyet Nguyen, A. Rand Andersen, E. Morten Skou, T. Lund, Dye stability and performances of dye-sensitized solar cells with different nitrogen additives at elevated temperatures—Can sterically hindered pyridines prevent dye degradation?, Sol. Energy Mater. Sol. Cells. 94 (2010) 1582-1590. https://doi.org/https://doi.org/10.1016/j.solmat.2010.04.076
[17] T. Lund, P.T. Nguyen, H.M. Tran, P. Pechy, S.M. Zakeeruddin, M. Grätzel, Thermal stability of the DSC ruthenium dye C106 in robust electrolytes, Sol Energy. 110 (2014) 96-104. https://doi.org/https://doi.org/10.1016/j.solener.2014.09.007
[18] T. Lund, P.T. Nguyen, T. Ruhland, Electrochemical grafting of TiO_2-based photo-anodes and its effect in dye-sensitized solar cells, J. Electroanal. Chem. 758 (2015) 85-92. https://doi.org/10.1016/j.jelechem.2015.10.021
[19] R.J. Hunter, Zeta potential in colloid science, Academic Press, San Diago, 1988.
[20] T.-Y. Tsai, H.-L. Wang, Y.-C. Chen, W.-C. Chang, J.-W. Chang, S.-Y. Lu, D.-H. Tsai, Noble metal-titania hybrid nanoparticle clusters and the interaction to proteins for photo-catalysis in aqueous environments, J. Colloid Interface Sci. 490 (2017) 802-811. https://doi.org/https://doi.org/10.1016/j.jcis.2016.12.001
[21] J.-T. Tai, C.-S. Lai, H.-C. Ho, Y.-S. Yeh, H.-F. Wang, R.-M. Ho, D.-H. Tsai, Protein–Silver Nanoparticle Interactions to Colloidal Stability in Acidic Environments, Langmuir. 30 (2014) 12755-12764. https://doi.org/10.1021/la5033465
[22] P.T. Nguyen, T.-D.T. Nguyen, V.S. Nguyen, D.T.-X. Dang, H.M. Le, T.-C. Wei, P.H. Tran, Application of deep eutectic solvent from phenol and choline chloride in electrolyte to improve stability performance in dye-sensitized solar cells, J Mol Liq 277 (2019) 157-162. https://doi.org/https://doi.org/10.1016/j.molliq.2018.12.114
[23] P.T. Nguyen, T.N. Nguyen, V.S. Nguyen, H.T. Nguyen, D.K. Thi Ngo, P.H. Tran, 1-Alkenyl-3-methylimidazolium trifluoromethanesulfonate ionic liquids: novel and low-viscosity ionic liquid electrolytes for dye-sensitized solar cells, RSC Advances. 8 (2018) 13142-13147. https://doi.org/10.1039/C7RA12904A
[24] V.A. Tran, T.T. Truong, T.A.P. Phan, T.N. Nguyen, T.V. Huynh, A. Agresti, S. Pescetelli, T.K. Le, A. Di Carlo, T. Lund, S.-N. Le, P.T. Nguyen, Application of nitrogen-doped TiO_2 nano-tubes in dye-sensitized solar cells, Appl Surf Sci. 399 (2017) 515-522. https://doi.org/https://doi.org/10.1016/j.apsusc.2016.12.125
[25] M.Q. Snyder, B.A. McCool, J. DiCarlo, C.P. Tripp, W.J. DeSisto, An infrared study of the surface chemistry of titanium nitride atomic layer deposition on silica from $TiCl_4$ and NH_3, Thin Solid Films. 514 (2006) 97-102. https://doi.org/10.1016/j.tsf.2006.03.013

[26] C. Shi, S. Dai, K. Wang, X. Pan, F. Kong, L. Hu, The adsorption of 4-tert-butylpyridine on the nanocrystalline TiO_2 and Raman spectra of dye-sensitized solar cells in situ, Vibrational Spectroscopy. 39 (2005) 99-105. https://doi.org/https://doi.org/10.1016/j.vibspec.2005.01.002
[27] T. Khoa Le, D. Flahaut, D. Foix, S. Blanc, H.K. Hung Nguyen, T.K. Xuan Huynh, H. Martinez, Study of surface fluorination of photocatalytic TiO_2 by thermal shock method, J. Solid State Chem. 187 (2012) 300-308. https://doi.org/https://doi.org/10.1016/j.jssc.2012.01.034
[28] M.G. Faba, D. Gonbeau, G. Pfister-Guillouzo, Core and valence spectra of titanium dichalcogenides TiX_2 (where X is O, S). Experimental and theoretical studies, J Electron Spectrosc 73 (1995) 65-80. https://doi.org/https://doi.org/10.1016/0368-2048(94)02285-2
[29] J.-C. Dupin, D. Gonbeau, P. Vinatier, A. Levasseur, Systematic XPS studies of metal oxides, hydroxides and peroxides, Phys. Chem. Chem. Phys. 2 (2000) 1319-1324. https://doi.org/10.1039/A908800H
[30] M. Göthelid, S. Yu, S. Ahmadi, C. Sun, M. Zuleta, Structure-Dependent 4-tert-butyl pyridine-Induced Band Bending at TiO_2 Surfaces, Int J Photoenergy 2011 (2011) 1-6. https://doi.org/10.1155/2011/401356
[31] L.K. Randeniya, A. Bendavid, P.J. Martin, E.W. Preston, Photoelectrochemical and Structural Properties of TiO_2 and N-Doped TiO_2 Thin Films Synthesized Using Pulsed Direct Current Plasma-Activated Chemical Vapor Deposition, J. Phys. Chem. C. 111 (2007) 18334-18340. https://doi.org/10.1021/jp075938u
[32] G. Ketteler, S. Yamamoto, H. Bluhm, K. Andersson, D.E. Starr, D.F. Ogletree, H. Ogasawara, A. Nilsson, M. Salmeron, The Nature of Water Nucleation Sites on TiO_2 (110) Surfaces Revealed by Ambient Pressure X-ray Photoelectron Spectroscopy, J. Phys. Chem. C. 111 (2007) 8278-8282. https://doi.org/10.1021/jp068606i
[33] H. Tiznado, F. Zaera, Surface Chemistry in the Atomic Layer Deposition of TiN Films from $TiCl_4$ and Ammonia, J. Phys. Chem. B. 110 (2006) 13491-13498. https://doi.org/10.1021/jp062019f
[34] T.M. Breault, B.M. Bartlett, Lowering the Band Gap of Anatase-Structured TiO_2 by Coalloying with Nb and N: Electronic Structure and Photocatalytic Degradation of Methylene Blue Dye, J. Phys. Chem. C. 116 (2012) 5986-5994. https://doi.org/10.1021/jp2078456
[35] T.-H. Kim, V. Rodríguez-González, G. Gyawali, S.-H. Cho, T. Sekino, S.-W. Lee, Synthesis of solar light responsive Fe, N co-doped TiO_2 photocatalyst by sonochemical method, Catal Today. 212 (2013) 75-80. https://doi.org/https://doi.org/10.1016/j.cattod.2012.09.014
[36] S. Sato, R. Nakamura, S. Abe, Visible-light sensitization of TiO_2 photocatalysts by wet-method N doping, Appl Catal A Gen. 284 (2005) 131-137. https://doi.org/https://doi.org/10.1016/j.apcata.2005.01.028
[37] S. Anandan, T.N. Rao, R. Gopalan, Y. Ikuma, Fabrication of Visible-Light-Driven N-Doped Ordered Mesoporous TiO_2 Photocatalysts and Their Photocatalytic Applications, J. Nanosci. Nanotechnol. 14 (2014) 3181-3186. https://doi.org/10.1166/jnn.2014.8530
[38] G. Yang, Z. Jiang, H. Shi, T. Xiao, Z. Yan, Preparation of highly visible-light active N-doped TiO_2 photocatalyst, J. Mater. Chem. . 20 (2010) 5301-5309. https://doi.org/10.1039/C0JM00376J
[39] P.T. Nguyen, V.S. Nguyen, T.A.P. Phan, T.N.V. Le, D.M. Le, D.D. Le, V.A. Tran, T.V. Huynh, T. Lund, Nicotinic acid as a new co-adsorbent in dye-sensitized solar cells, Appl Surf Sci. 392 (2017) 441-447. https://doi.org/https://doi.org/10.1016/j.apsusc.2016.09.064

[40] P.E. Hansen, P.T. Nguyen, J. Krake, J. Spanget-Larsen, T. Lund, Dye-sensitized solar cells and complexes between pyridines and iodines. A NMR, IR and DFT study, Spectrochimica Acta A. 98 (2012) 247-251. https://doi.org/https://doi.org/10.1016/j.saa.2012.08.006
[41] P.J. Cameron, L.M. Peter, S. Hore, How Important is the Back Reaction of Electrons via the Substrate in Dye-Sensitized Nanocrystalline Solar Cells?, J. Phys. Chem. B. 109 (2005) 930-936. https://doi.org/10.1021/jp0405759
[42] C.D. Christiansen, L.A. Sørensen, T. Lund, Modification of fluorine-doped tin oxide-electrodes by electrochemical reduction of di(4-nitrophenyl)iodonium tetrafluoroborate - And its application as a photo-anode in dye-sensitized solar cells, J. Electroanal. Chem. 809 (2018) 44-51. https://doi.org/https://doi.org/10.1016/j.jelechem.2017.12.050
[43] B.A. Gregg, F. Pichot, S. Ferrere, C.L. Fields, Interfacial Recombination Processes in Dye-Sensitized Solar Cells and Methods To Passivate the Interfaces, J. Phys. Chem. B. 105 (2001) 1422-1429. https://doi.org/10.1021/jp003000u
[44] J.M. Cole, G. Pepe, O.K. Al Bahri, C.B. Cooper, Cosensitization in Dye-Sensitized Solar Cells, Chemical Reviews. 119 (2019) 7279-7327. https://doi.org/10.1021/acs.chemrev.8b00632
[45] X. Liu, X. Ding, Y. Ren, Y. Yang, Y. Ding, X. Liu, A. Alsaedi, T. Hayat, J. Yao, S. Dai, A star-shaped carbazole-based hole-transporting material with triphenylamine side arms for perovskite solar cells, Journal of Materials Chemistry C. 6 (2018) 12912-12918. https://doi.org/10.1039/C8TC04191A